18th Australasian Fluid Mechanics Conference
Launceston, Australia
3-7 December 2012

Experimental Modelling of Steady Hydrofoil Fluid-Structure Interaction

P.A. Brandner and B.W. Pearce

Australian Maritime College

University of Tasmania, Launceston, Tasmania 7250, Australia

Abstract

Static hydroelastic behaviour of two geometrically identical flexible metal hydrofoils of Aluminium and Stainless Steel are investigated in a water tunnel. The hydrofoils are of unswept trapezoidal planform, aspect ratio 3.33, NACA 0009 section and were oriented vertically in the water tunnel mounted on a force balance through the test section ceiling. Forces and deflections were measured at several chord-based Reynolds numbers up to 10^6 and incidences beyond stall. Hysteresis and the effect of test section ceiling boundary layer thickness were investigated. Prestall forces where observed to be Reynolds number dependent for low values but became independent at 0.8×10^6 and greater. Tip deflections up to 4.5% of span were measured for the Aluminium hydrofoil. Forces and deflections were observed to be stable up to stall. Non-dimensional tip deflections of both hydrofoils were found to be independent of incidence. Forces for both hydrofoils compare closely for all incidences and Reynolds numbers tested, within uncertainties, showing these to be independent of deformation.

Introduction

The present work is motivated by the desire to develop so called "hydro-elastically" tailored marine propellers and hydrofoils using composite materials to improve hydrodynamic performance. Hydroelastic tailoring in the present context may be defined as the intentional use of structural and material properties to improve hydrodynamic performance in a broad sense including both static and dynamic behaviour. That is, structures may be designed to deform under increasing quasi-steady or dynamically varying applied loads to give improved hydrodynamic performance compared with a 'rigid' or relatively stiff structure. It is envisaged that propellers maybe designed with improved propulsive efficiency as well as reduced unsteady or harmonic force components, vibration and noise emissions. For naval ships, where it is most desirable to reduce vibration and harmonic excitation due to spatial and temporal variations of the inflow to propellers and control surfaces, composites may offer significant advantages over traditional materials.

Traditionally marine propulsion and control equipment have been manufactured in metal particularly using nickel-aluminium bronze or stainless steel. These conventional materials offer the advantages of being homogeneous and isotropic for the purposes of modelling their structural behaviour. There is also extensive experience of their manufacture and use in the challenging marine environment for both civilian and naval applications. Composite materials are continuously being developed and are now used extensively in aeronautical applications with limited use to date for ship hull and superstructure applications [13]. Their use for propellers and control surfaces has to date been more limited due to the technical difficulties of designing such devices and the uncertainties over their serviceability and reliability. Composites do, however, offer advantages over traditional materials including reduced weight, corrosion resistance and the potential for hydrodynamic performance improvement through hydroelastic tailoring [13, 7, 12, 11].

With increasing sophistication of experimental and numerical modelling of the turbulent flow about the after-bodies of ships and submarines the complex nature of the flow in which control surfaces and propellers must operate is being revealed [8, 2, 1]. These flows are both spatially and temporally non-uniform and need to be understood and characterised in order that more efficient propulsion and control equipment may be developed. Classically the problem of marine propellers has been analysed considering the inflow to consist of spatial non-uniformity of the mean velocity components only, with the effects of turbulence and temporal fluctuations ignored [4, 9, 6]. Additionally, the complex problem of the dynamic or Fluid-Structure Interaction (FSI) of the deforming hydrofoils or blades with the turbulent flow field must be modelled and understood. Significant work has been done on the problem of the composite propeller blade and spatially uniform or non-uniform potential flow [12, 10] showing the complexity in the structural modelling required for composites.

To gain basic insight into the FSI problem, as it relates to propellers and control surfaces, experiments are planned of a simple unsteady flow about a flexible three-dimensional hydrofoil. The use of a hydrofoil significantly reduces the complexity of models and the experimental setup required compared with that for propellers. Several hydrofoils of identically simple geometry but of differing materials will be tested. An unsteady flow that provides a simplified analogy to spatial/temporal non-uniformity of inflow to propellers or control surfaces is impulsive or periodic variation of incidence. This method eliminates the difficulty of generating unsteadiness in the upstream flow. This arrangement is also compatible with setting up relatively simple numerical models. To also maintain relative simplicity in corresponding numerical modelling, metals and a simple composite layup have been chosen for hydrofoil materials for experiments. A new dynamic force balance has been developed capable of measuring unsteady forces while the hydrofoil undergoes sinusoidal or impulsive incidence variation over a suitable range of frequencies and amplitudes.

The present work reports on development of experimental techniques and results of static hydroelastic testing of two metal hydrofoils of Aluminium (Al) and Stainless Steel (SS). Forces and deflections are measured for a range of Reynolds numbers, *Re* and incidences, α. From these data the effect of static flexibility can be assessed including effects on steady and unsteady forces and hysteresis. These results also serve as baseline data for later comparison with planned unsteady experiments.

Experimental Overview

Model Hydrofoil Details

Hydrofoil geometry and physical/mechanical properties have been selected based on the requirements discussed above for modelling of static and dynamic conditions typical of those experienced by propellers and hydrofoils operating in ship or submarine wakes. The selected geometry is an upright or unswept trapezoidal planform with 0.3 m span, 0.12 m base chord,

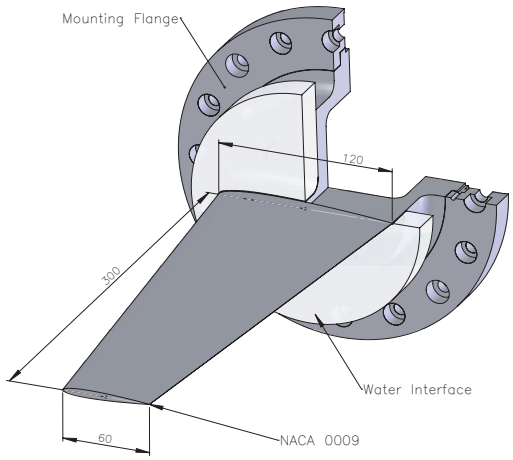

Figure 1: Arrangement, geometry and dimensions of model hydrofoils showing mounting flange and fairing disk where the models penetrate the tunnel wall (dimensions in mm).

0.06 m tip chord (aspect ratio 3.33) and NACA 0009 section, as shown in Figure 1. An unswept geometry was deliberately chosen to consider bending deformations only for this study. The scale of the models was chosen to be compatible with the water tunnel test section with the span being half the cross-section dimension and the chord sufficient to obtain chord-based *Re* values of at least 1×10^6. SS and Al were chosen as suitable materials in terms of properties and being practical to manufacture. Table 1 summarises the material and structural properties. Al and SS have similar ratios of elastic modulus, E to density, ρ_H such that for the same geometry they have virtually identical natural frequencies in air. The thickness chosen gives 100 Hz first mode natural frequency, f_n in air (from impact test) and 42 and 62 Hz for the SS and Al models respectively in water (from added mass estimate [3]). These values were chosen as a compromise between the level of flexibility and response and maintaining a reasonable margin against hydroelastic instability phenomena. The ratio of hydrofoil to liquid density or mass ratio, ρ_H/ρ_L differs by about a factor of 3 between the two materials. Both models were machined from solid billets with an integral mounting flange, as shown in Figure 1, to 0.8 μm surface finish and 0.1 mm surface tolerance. The Al model was anodised to a thickness of about 5 μm. The maximum mean load permissible was set at 1 kN providing appropriate margins against structural damage.

Experimental Setup

Experiments were carried out in the Cavitation Research Laboratory (CRL) water tunnel at the Australian Maritime College (AMC). The tunnel test section is 0.6 m square by 2.6 m long in which the operating velocity and pressure ranges are 2 to 12 m/s and 4 to 400 kPa absolute respectively. The tunnel volume is 365 m^3 with demineralised water (conductivity of order 1 μS/cm). The tunnel has ancillary systems for rapid degassing and for continuous injection and removal of nuclei and large volumes of incondensable gas. A detailed description of the facility is given in [5]. The test section velocity is measured from one of two (high and low range) Siemens Sitransp differential pressure transducers models 7MF4433-1DA02-2AB1-Zand 7MF4433-1FA02-2AB1-Z (measuring the calibrated contraction differential pressure) with estimated precisions of 0.007 and 0.018 m/s respectively.

The models were mounted on a 6-component force balance extending vertically into the flow through a 0.16 m diameter penetration on the tunnel ceiling. The 0.16 m diameter penetration was made fair (to 50 μm) using a disk mounted, in this case, on the hydrofoil (see Figure 1) or measurement side of the balance with a typical 0.5 mm radial clearance to avoid interference with the force measurement. Of the total load vector measured using the balance, mean and unsteady components of lift, drag and pitching moment are presented. Spanwise forces and roll/yaw moments are not considered as they may be contaminated by the wall pressure distribution acting on the disk using this setup. Data where sampled at 1 kHz for durations from 10 to 30 s for the highest to lowest *Re* values respectively.

Hydrofoil Model	1	2
Material	SS(316L)	AL(6061 T6)
E, GPa	193	69
ρ_H, kg/m^3	7900	2700
E/ρ_H, MNm/kg	25.3	25.6
f_n(air), Hz	100	100
f_n(water), Hz	62	42
ρ_H/ρ_L	7.9	2.7
Max allow lift, kN	1	1

Table 1: Summary of material and structural properties of Al and SS model hydrofoils.

Measurements were made at two streamwise locations (0.7 and 1.3 m from the test section entrance) to test the effect of varying ceiling boundary layer thickness. The balance is calibrated by a least squares fit between a basis vector loading cycle and the 6 outputs giving a 6×6 matrix from which estimated precision on all components is less than 0.1%. Forces were measured at mean chord-based *Re* values (mean chord = 0.09 m) of 0.2, 0.4, 0.6, 0.8 and 1.0×10^6, at α values beyond stall or up to the estimated maximum load of 1 kN. Hydrofoil incidence is adjusted using the balance automated indexing system incremented in 0.5° steps. The absolute position of the force balance incidence indexing system is less than 0.1° and the incremental precision is less than 0.001°. For hysteresis tests a 0.05° incidence correction is applied for backlash in the indexing mechanism. The tunnel was pressureised up to 200 kPa for all tests to prevent cavitation occurence.

Tip deflections were measured using cross correlation of still photographs of the hydrofoil end faces before and after loading. The correlation was made on contrasting targets located near the leading and trailing edges of the end faces (Figure 5). Photographs were taken using a Canon EOS 50D 35 mm digital SLR camera with a Canon EF 24-70 mm lens using natural lighting (image resolution 4752×3168). The images were calibrated from a gird located in the plane of the hydrofoil tip before installing the models. Deflections were measured for all Reynolds numbers mentioned above up to 10° incidence in 2° increments. The error estimate from this method for the worst case of the SS hydrofoil varies from about 10% at lowest incidence to 0.5% at the maximum incidence tested.

Results

The measured lift, L drag, D and pitching moment, M are presented as dimensionless coefficients, $C_L = 2L/(\rho_L U_\infty^2 sc)$, $C_D = 2D/(\rho_L U_\infty^2 sc)$ and $C_M = 2M/(\rho_L U_\infty^2 sc^2)$, respectively where U_∞ is the freestream velocity, s the hydrofoil span and c the mean chord. The coordinate system origin for the measured forces is located on the centreplane of the hydrofoil at midchord. The measured deflections are nondimensionalised, $y' = yEI/(F_n s^3)$, where I is the base section second moment of

area and F_n the hydrodynamic force normal to the chord line.

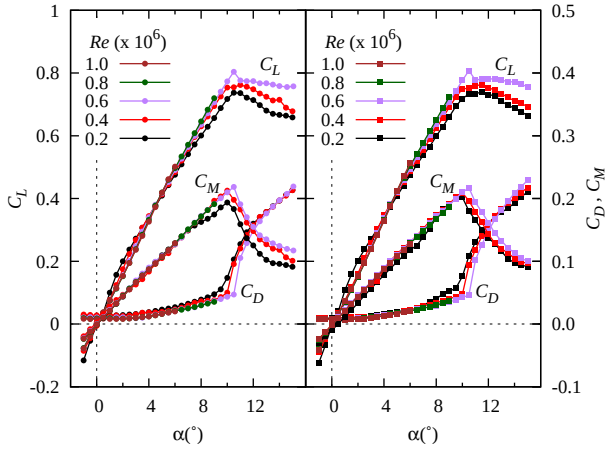

Figure 2: Lift, drag and pitching moment coefficients with incidence for SS (left) and Al (right) hydrofoil models located 0.7 m from test section entrance, for several *Re* values. Pre-stall lift forces are dependent on *Re* at low values but become independent for values of 0.8×10^6 and greater. Forces and moments for both hydrofoil models appear to compare closely for all *Re* and α values despite differences in deflection.

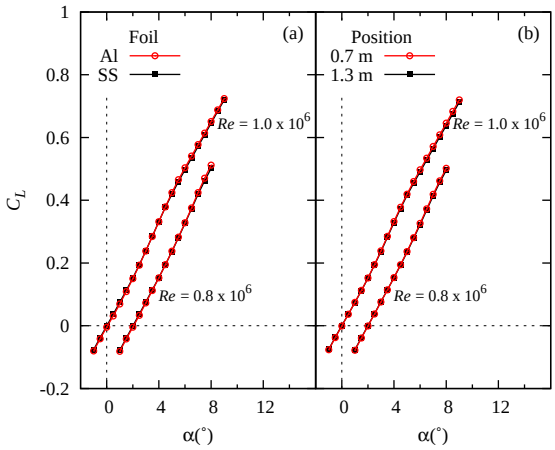

Figure 3: (a) Comparison of lift forces with incidence for SS and Al hydrofoils located 0.7 m from test section entrance at higher Reynolds numbers showing independence of *Re* and material despite different deflections. (b) Comparison of SS hydrofoil at 0.7 and 1.3 m from test section entrance at the higher Reynolds numbers showing differences of less than 1% due to differences in boundary layer thickness. The boundary layer thickness, δ_{99} at the 0.7 and 1.3 m positions are about 19 and 26 mm respectively. (Plots are staggered by 2°).

Forces

Mean coefficients of lift, drag and pitching moment for the SS and Al hydrofoils with the models located 0.7 m from the test section entrance are presented in Figure 2. For the lowest three *Re* values the incidence was incremented beyond stall to 15° without exceeding the maximum lift of 1 kN. Whereas for *Re* = 0.8 and 1.0×10^6 incidences were limited to 6 and 9° respectively to avoid exceeding the limit. Forces and moments for both hydrofoil models appear to compare closely for all *Re* and α values. Stall occurs at nominally 10.5° incidence for the three *Re* values tested for both models. Pre-stall lift forces show a dependence on *Re* for low values due presumably to laminar flow effects but become independent for *Re* = 0.8×10^6 and greater for the incidence range tested. Similar behaviour is evident in the drag and pitching moment coefficients. The lift coefficients for the two largest *Re* values are replotted in Figure 3a showing the close comparison demonstrating their independence of *Re* and material despite the difference in deflections discussed in detail below. A slight difference in lift coefficient between the two materials is just evident at the highest *Re* and incidence indicating that for greater values differing deflections may affect the lift, although this would increase stresses beyond typical working values.

Figure 3b shows the comparison of lift forces measured for the SS hydrofoil at two streamwise locations in the test section showing the effect of varying ceiling (or hydrofoil base) boundary layer thickness on the lift to be less than 1%. The boundary layer thickness (for 99%U_∞), at the 0.7 and 1.3 m positions are about 19 and 26 mm respectively.

Figure 4 presents forces and moments from a complete incidence loop for both hydrofoil materials for *Re* = 0.6×10^6 showing that the presumed complex laminar flow effects occurring at low *Re* values essentially do not cause any hysteresis effects in the forces.

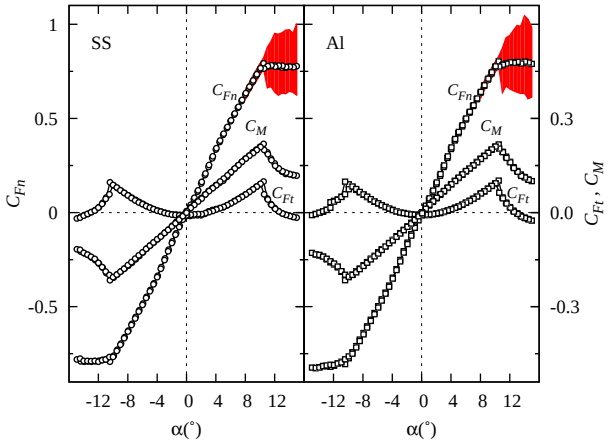

Figure 4: Foil chordwise normal (C_{Fn}) & transverse (C_{Ft}) forces and pitching moment measurements taken over a full incidence cycle ($\alpha = 0°$ to $+14°$ to $-14°$ to $0°$) for SS and Al hydrofoils indicating no hysteresis ($Re = 0.6 \times 10^6$). Also shown is the envelope of maximum and minimum C_{Fn} with positive incidence.

Also shown in Figure 4 is the envelope of maximum and minimum chordwise normal force with incidence for the SS and Al hydrofoils. The envelope shows the unsteady forces are less than 4% of the mean for all incidences up to stall after which they suddenly increase up to 30%. The envelope for the Al is slightly greater than the SS which could be attributed to the lower stiffness, and therefore greater defections of the Al. Spectra of the normal forces at pre-stall incidences show a level response up to a peak at about 110 and 120 Hz for the SS and Al hydrofoils respectively. This difference in balance response is due to the difference in mass between the two models. For post-stall incidences another lower peak in the spectra appears at about 45 and 55 Hz for the Al and SS hydrofoils respectively. These reflect the balance response to the onset of unsteady flow with stall and the excitation of the models first mode. These frequencies are similar to those predicted for the hydrofoils alone listed in the experimental overview.

Deformations

Figure 5 shows a sample image pair for the largest deflections measured of the Al hydrofoil at *Re* = 0.8×10^6 and 6° incidence. These images were taken using stroboscopic illumination to see

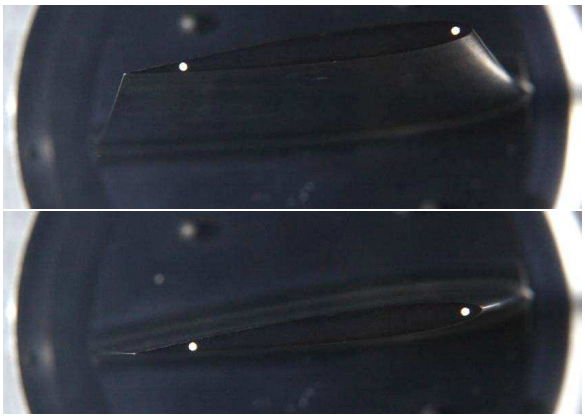

Figure 5: Images of the Al hydrofoil tip with and without flow at 6° incidence and $Re = 1.0 \times 10^6$ showing test targets for image cross-correlation to derive tip deflection.

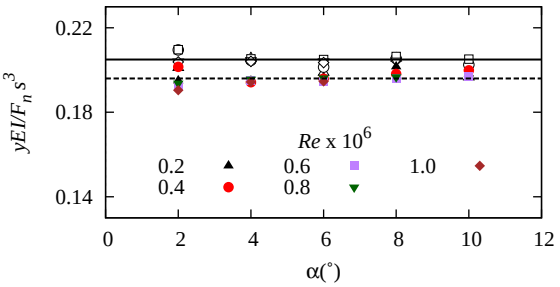

Figure 6: Comparison of dimensionless tip deflections for SS (open symbols) and Al (coloured symbols) hydrofoils showing a difference of 4% which could be attributable to errors in modulus estimates.

the hydrofoil whereas the actual images used for cross correlation to measure the deflection where taken using natural lighting. This technique resulted in an essentially black background with only the white markers showing providing optimum contrast for the cross correlation. As only still images were taken this technique was limited to pre-stall incidences where there was no observable hydrofoil vibration.

Maximum deflections were measured at $Re = 1.0 \times 10^6$ and 6° incidence of 4.9 mm and 13.4 mm for the SS and Al hydrofoils respectively. No twist was resolved within the precision of the method used suggesting it is small enough to be negligible. The force measurements tend to confirm this as they show no difference between the two materials despite the much larger deflections (and potentially the twist) of the Al hydrofoil.

On this basis dimensionless deflections should be the same for both materials, as shown in Figure 6. The results show virtually no dependence on incidence or *Re* allowing for greater error at the lower incidences and *Re*. The mean values of 0.204 and 0.196 indicated on Figure 6 for the SS and Al hydrofoils show a difference of 3.9% which could be attributable to errors in the assumed modulus values (193 and 69 GPa). These values of about 0.2 compare with, for example, 0.125 for a uniformly loaded cantilever of uniform cross-section.

Conclusions

Static hydroelastic behaviour of two geometrically identical flexible metal hydrofoils of Aluminium and Stainless Steel were investigated in a water tunnel. Pre-stall forces where observed to be Reynolds number dependent for low values but became independent at 0.8×10^6 and greater. Forces and deflections were observed to be stable up to stall. Forces for both hydrofoils compare closely for all incidences and Reynolds numbers tested, within uncertainties, showing these to be independent of deformation. Non-dimensional tip deflections of both hydrofoils were found to be independent of incidence. The dimensionless constant of proportionality between deflections and hydrofoil loading, geometry and material properties was found to differ by about 4% which could be attributable to errors in modulus estimates.

Acknowledgements

The authors wish to acknowledge the support of the Defence Science and Technology Organisation, the Australian Maritime College and the US Office of Naval Research Global (Dr Ki-Han Kim, program manager) through NICOP S&T Grant No. N62909-11-1-7013.

References

[1] Alin, N., Bensow, R., Fureby, C., Huuva, T. and Svennberg, U., Current capabilities of DES and LES for submarines at straight course, *Journal of Ship Research*, **54**, 2010, 184–196.

[2] Andersen, P., Kappel, J. J. and Spangenberg, E., Aspects of propeller developments for a submarine, in *First International Symposium on Marine Propulsors - SMP09*, editors K. Koushan and S. Steen, Trondheim, Norway, 2009.

[3] Blevins, R. D., *Formulas for Natural Frequency & Mode Shape*, Van Nostrand Reinhold Co., New York, 1979.

[4] Boswell, R. J. and Miller, M. L., Unsteady propeller loading-measurement, correlation with theory, and parametric study, Report 2625, David W Taylor Naval Ship Research and Development Center, 1968.

[5] Brandner, P. A., Lecoffre, Y. and Walker, G. J., Design considerations in the development of a modern cavitation tunnel, in *16th Australasian Fluid Mechanics Conference*, Crown Plaza, Gold Coast, Australia, 2007, 630–637.

[6] Breslin, J. P. and Andersen, P., *Hydrodynamics of Ship Propellers*, Cambridge Ocean Technology Series, Cambridge University Press, Cambridge, 1994.

[7] Chen, B. Y.-H., Neely, S. K., Michael, T. J., Gowing, S., Szwerc, R. P., Buchler, D. and Schult, R., Design, fabrication and testing of pitch-adapting (flexible) composite propellers, in *Propellers/Shafting 2006*, Williamsburg, Virginia, 2006.

[8] Fureby, C., ILES and LES of complex engineering turbulent flows, *Journal of Fluids Engineering*, **129**, 2007, 1514–1523.

[9] Kerwin, J. E., Marine propellers, *Annual Review of Fluid Mechanics*, **18**, 1986, 367–403.

[10] Liu, Z. and Young, Y. L., Utilization of bendtwist coupling for performance enhancement of composite marine propellers, *Journal of Fluids and Structures*, **25**, 2009, 11021116.

[11] Miller, R., Kim, S.-E. and Lee, S. W., A computational framework for fluid-structure interaction on flexible propellers involving large deformation, in *28th Symposium on Naval Hydrodynamics*, Pasadena, California, 2010.

[12] Motley, M., Liu, Z. and Young, Y., Utilizing fluidstructure interactions to improve energy efficiency of composite marine propellers in spatially varying wake, *Composite Structures*, **90**, 2009, 304–313.

[13] Mouritz, A., Gellert, E., Burchill, P. and Challis, K., Review of advanced composite structures for naval ships and submarines, *Composite Structures*, **53**, 2001, 22–41.